SUPPORTING INFORMATION

The allosteric control mechanism of bacterial glycogen biosynthesis disclosed by cryoEM

Javier O. Cifuente[1,§,*], Natalia Comino[1,§], Cecilia D'Angelo[1], Alberto Marina[1], David Gil-Carton[1], David Albesa-Jové[1], Marcelo E. Guerin[1,2,*]

[1]Structural Biology Unit, CIC bioGUNE, Bizkaia Technology Park, 48160 Derio, Spain.
[2]IKERBASQUE, Basque Foundation for Science, 48013, Bilbao, Spain.

*To whom correspondence may be addressed: Javier O. Cifuente and Prof. Marcelo E. Guerin, Structural Biology Unit, CIC bioGUNE, Bizkaia Technology Park, 48160 Derio, Spain, Tel +34 944 061 309, E-mail: Javier O. Cifuente, jcifuente@cicbiogune.es; E-mail: Marcelo E. Guerin, mrcguerin@cicbiogune.es

TABLE OF CONTENTS

SUPPLEMENTARY TABLES

Table S1. Fitting parameters for ITC data for four sites ATP sequential binding model.

	*Ec*AGPase-FBP vs ATP		*Ec*AGPase-AMP vs ATP	
Binding site	K_D (M)	ΔH (kcal/mol)	K_D (M)	ΔH (kcal/mol)
1	$2.30 \times 10^{-9} \pm 6.48 \times 10^{-10}$	-7.93 ± 1.60	$1.53 \times 10^{-4} \pm 2.22 \times 10^{-3}$	-28.5 ± 676
2	$4.20 \times 10^{-7} \pm 4.36 \times 10^{-6}$	-2.85 ± 25.7	$1.24 \times 10^{-3} \pm 1.94 \times 10^{-1}$	1.62 ± 1130
3	$3.30 \times 10^{-10} \pm 3.42 \times 10^{-9}$	-0.86 ± 24.2	$84.7 \times 10^{-9} \pm 21.6 \times 10^{-1}$	21.6 ± 1360
4	$3.37 \times 10^{-4} \pm 1.15 \times 10^{-6}$	-29.9 ± 4.32	$1.03 \times 10^{-3} \pm 1.51 \times 10^{-1}$	-40.4 ± 7260

SUPPLEMENTARY FIGURES

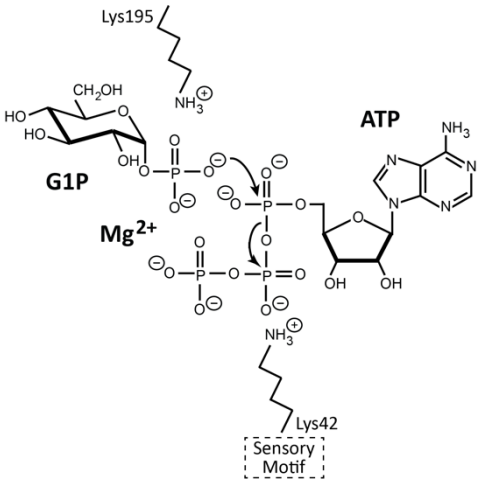

Figure S1. The catalytic mechanism of *Ec*AGPase. The α-phosphate from G1P must face the α-phosphate from ATP in the right geometry for the nucleophilic attack to take place. The positioning and the activation of the intervening phosphate groups relies on: (i) the interaction of the PO_4^{3-} groups with the Mg^{2+} bound to the putative aspartate dyad, (ii) the anchoring of the ATP to the G-rich loop, with the γPO_4^{3-} interacting with a highly conserved arginine, Arg32 in *Ec*AGPase, (iii) the interaction with two highly conserved catalytic lysines, Lys42 for ATP and Lys195 for G1P in *Ec*AGPase, which polarize the phosphates groups to facilitate the nucleophilic reaction. Finally, structural evidences in related enzymes support the ordered release of PPi first and ADPG second after the catalysis. The PPi molecule appears more solvent exposed and ready to leave the active site while the sugar phosphate is buried in the active site.

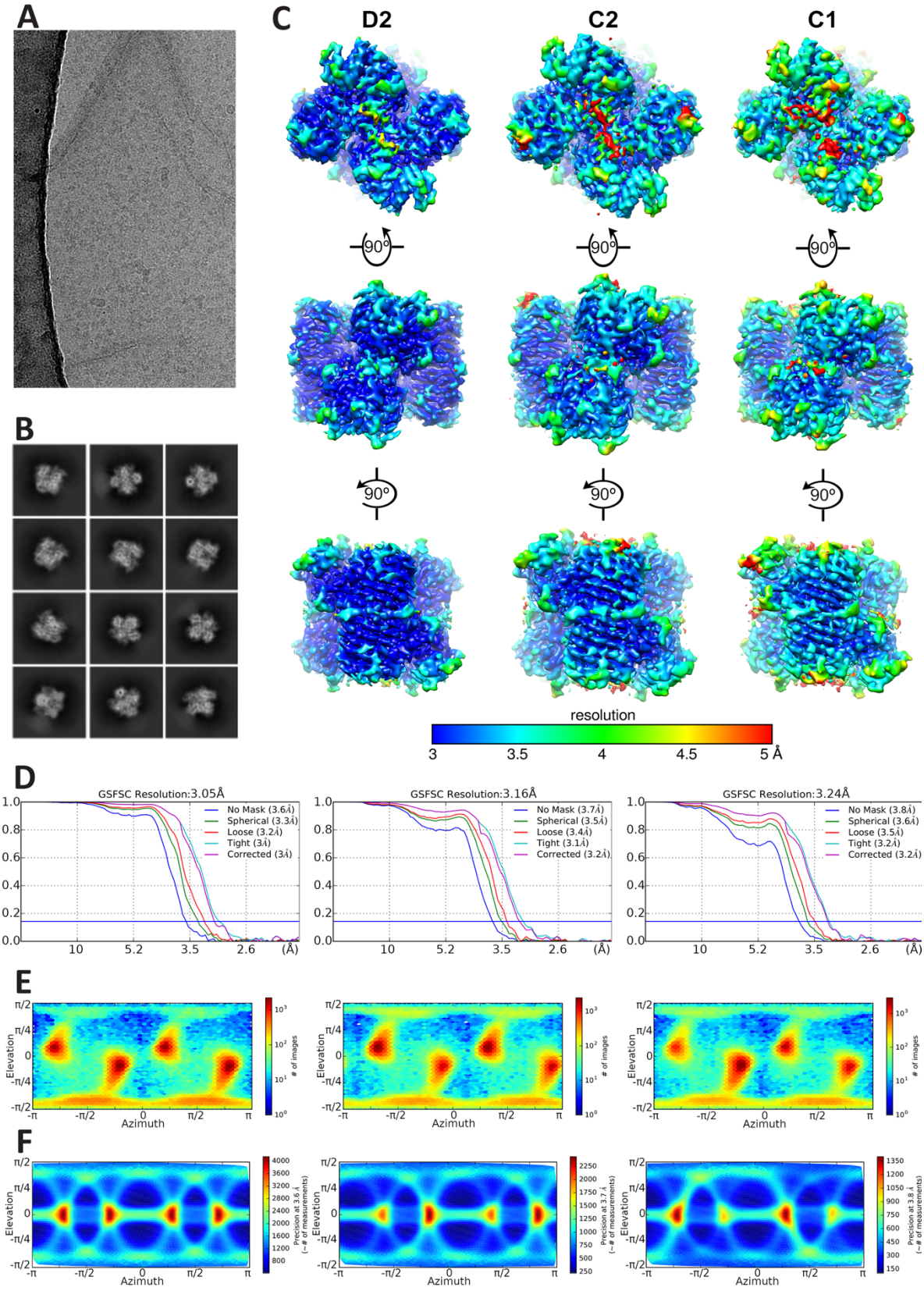

Figure S2. The *Ec*AGPase-FBP complex. (**A**) Micrograph detail. (**B**) Representative 2D classes. (**C**) Overall view of the single-particle reconstructions of *Ec*AGPase-FBP complex in D2, C2 and C1 symmetries, colored according to local resolution. (**D**) From left to right, the FSC plots of the *Ec*AGPase-FBP for the D2, C2 and C1 reconstructions. (**E**) From left to right, direction distribution of *Ec*AGPase-FBP particle images in the D2, C2 and C1 reconstructions. (**F**) From left to right, posterior precision plots for the *Ec*AGPase-FBP particle images in the D2, C2 and C1 reconstructions.

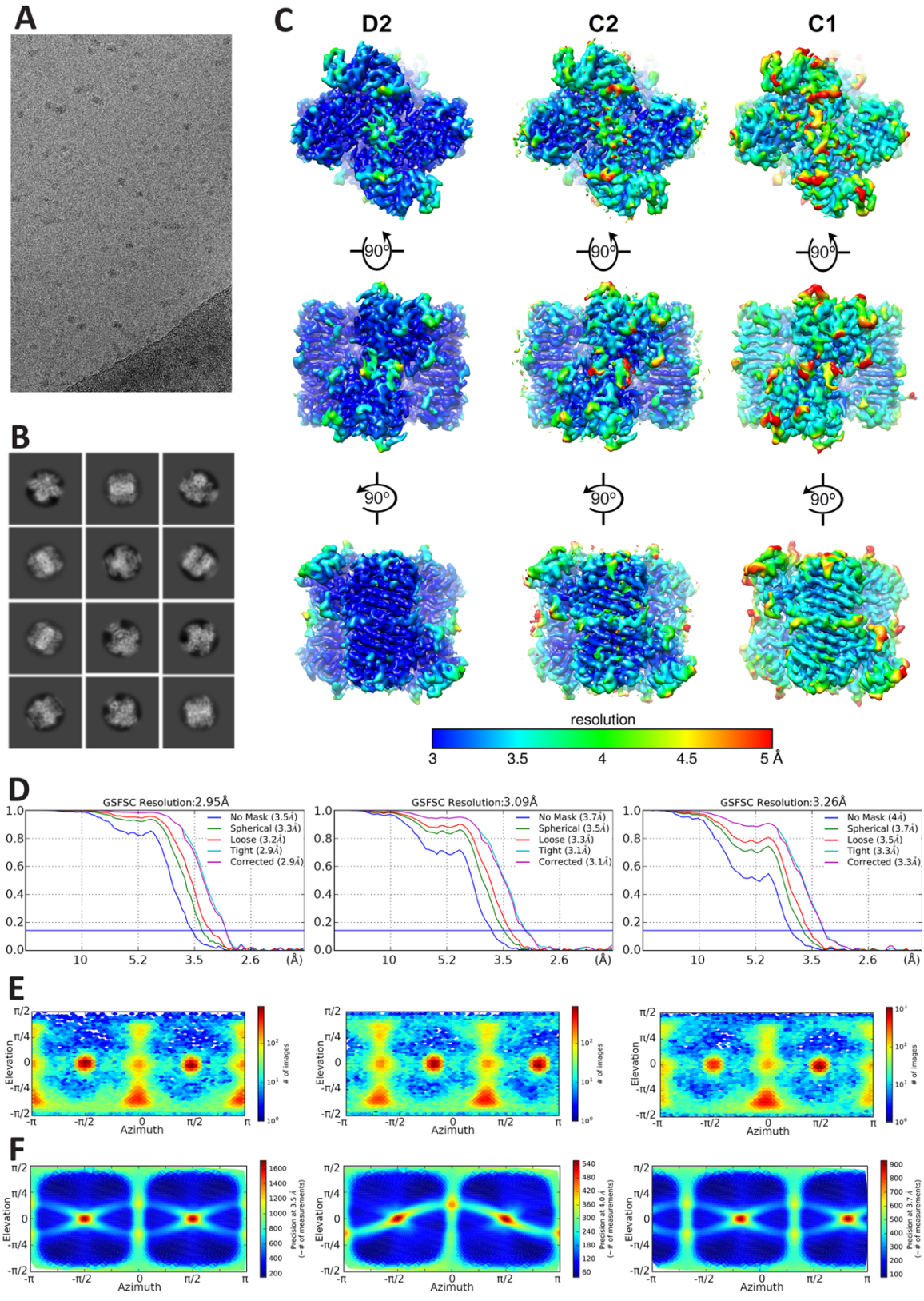

Figure S3. The *Ec*AGPase-AMP complex. (**A**) Micrograph detail. (**B**) Representative 2D classes. (**C**) Overall view of the single-particle reconstructions of *Ec*AGPase-AMP complex in D2, C2 and C1 symmetries, colored according to local resolution. (**D**) From left to right, the FSC plots of the *Ec*AGPase-AMP for the D2, C2 and C1 reconstructions. (**E**) From left to right, direction distribution of *Ec*AGPase-AMP particle images in the D2, C2 and C1 reconstructions. (**F**) From left to right, posterior precision plots for the *Ec*AGPase-FBP particle images in the D2, C2 and C1 reconstructions.

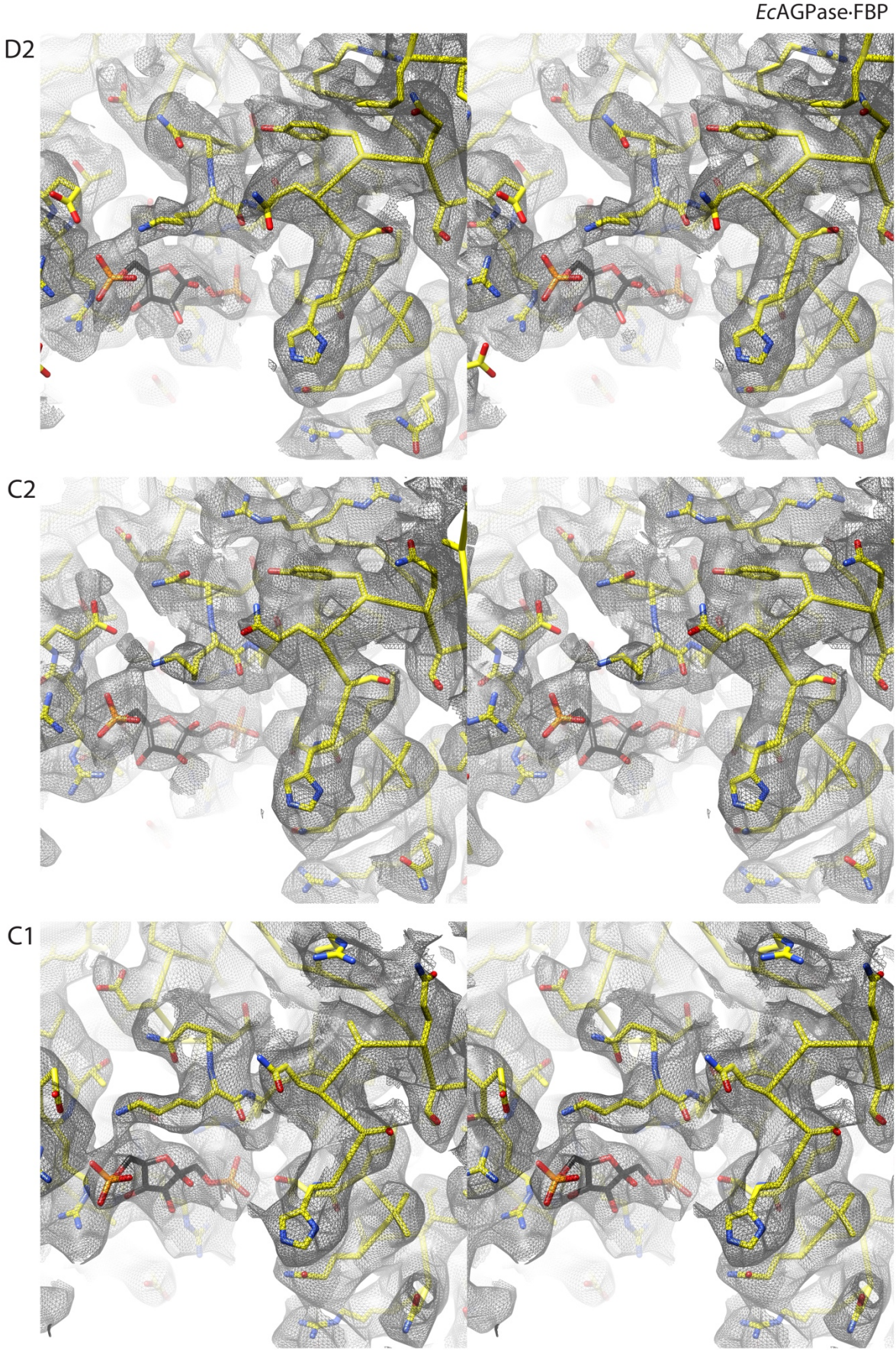

Figure S4. Local stereo views of the *Ec*AGPase-FBP model and maps. From top to bottom, a closed view of FBP ligand and the surrounding region of the D2, C2 and C1 map reconstructions and their corresponding models represented as yellow sticks.

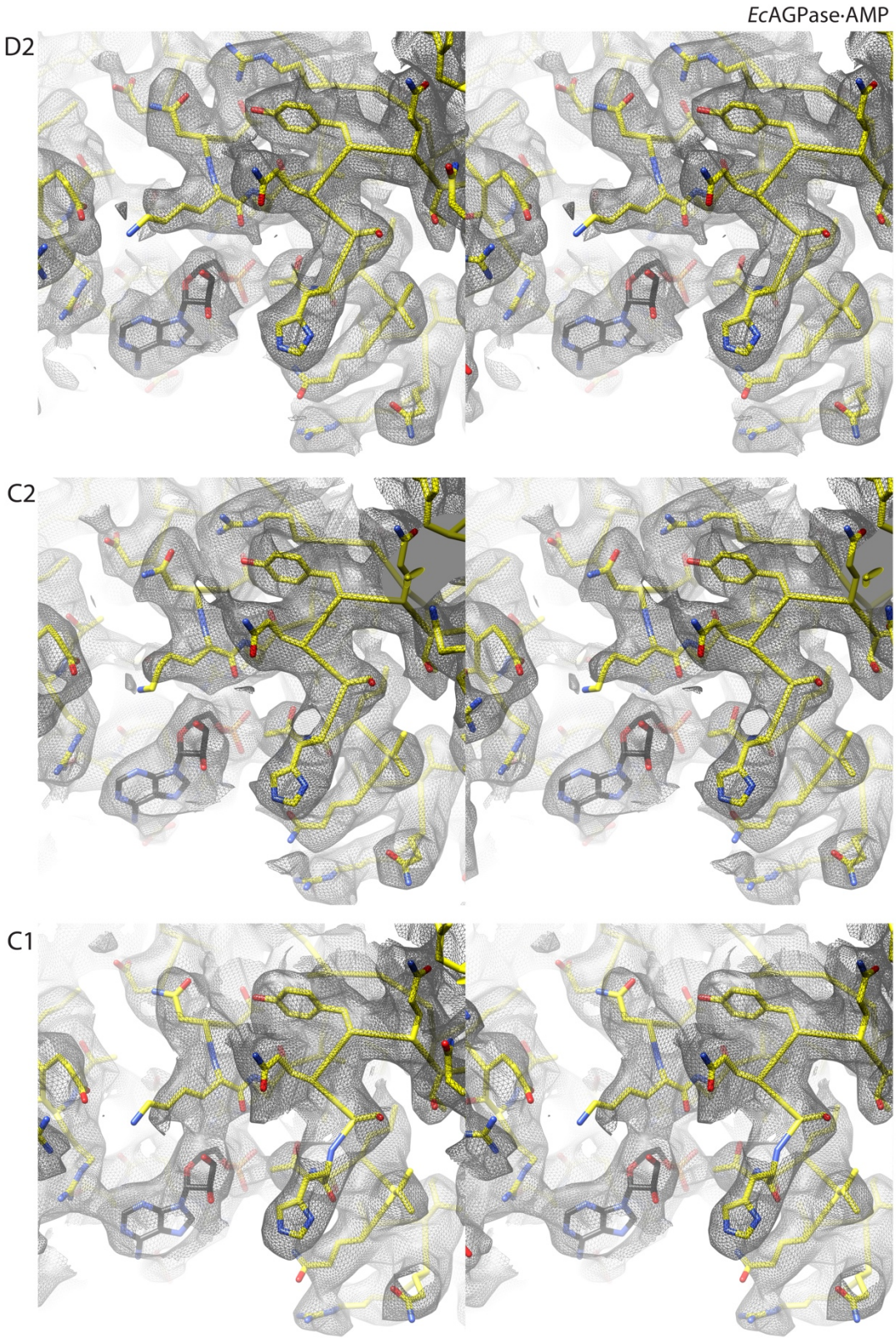

Figure S5. Local stereo views (crossed-eyes) of the *Ec*AGPase-AMP model and maps. From top to bottom, a closed view of AMP ligand and the surrounding region of the D2, C2 and C1 map reconstructions and their corresponding models represented as yellow sticks.

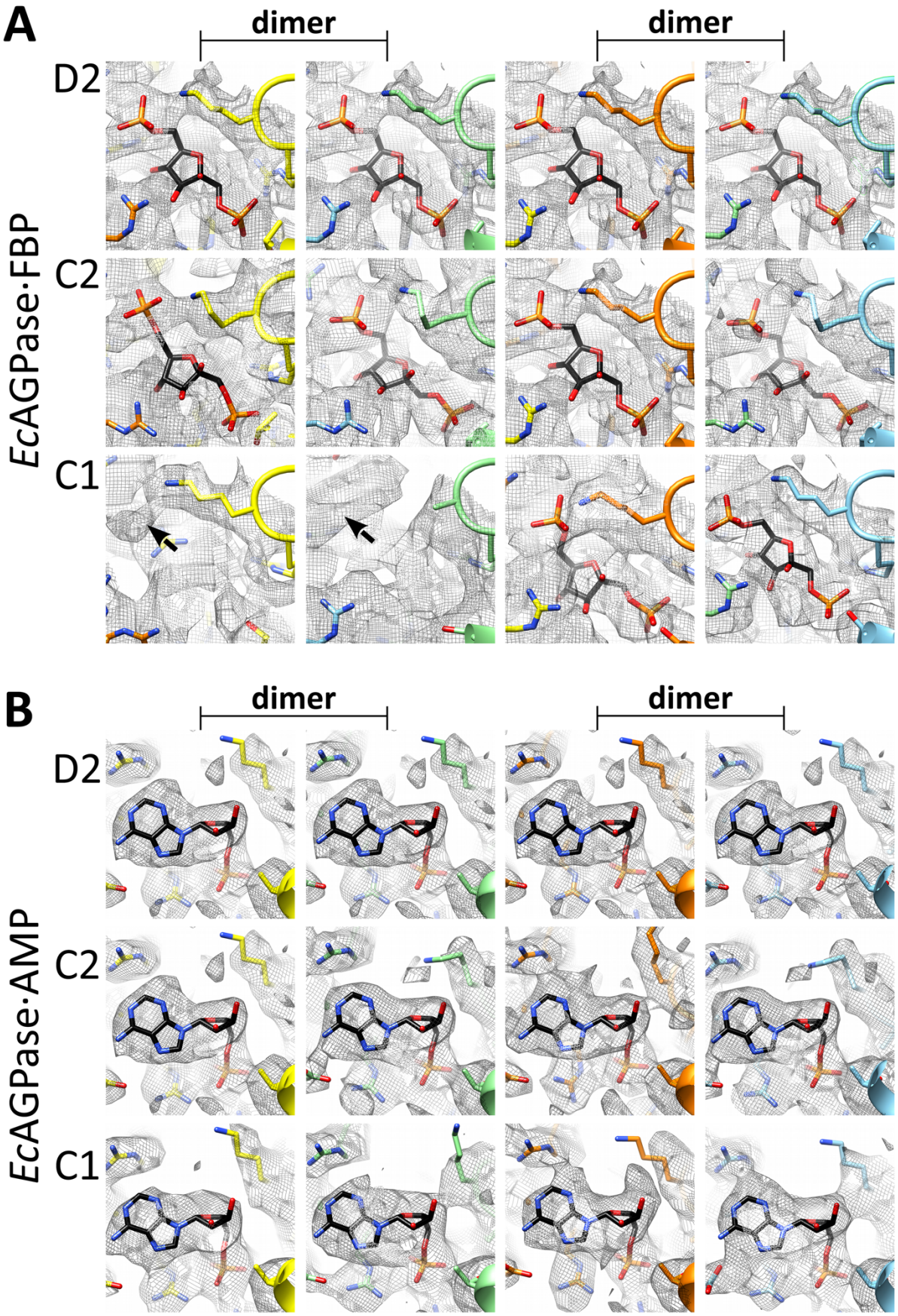
A
dimer
dimer
D2
C2
C1
EcAGPase·FBP
B
dimer
dimer
D2
C2
C1
EcAGPase·AMP

Figure S6. Electron density in the regulatory sites in *Ec*AGPase complexes. Picture gallery showing the electron density at the allosteric sites in the different symmetries. The color code of the different protomers is equivalent to that observed in Figure S6. (**A**) Close view of the regulatory cleft of the *Ec*AGPase·FBP complex in different symmetries. Note the equivalence of sites when D2 symmetry is imposed. Differences in the electron density between different sites appear evident with the imposition of the C2 symmetry. Note the impossibility to model FBP in the two sites in C1, although residual density appears (arrows). (**B**) Close view of the regulatory cleft in the *Ec*AGPase·AMP complex, in different symmetries, D2, C2 and C1. Note the consistency of density corresponding to AMP regardless of the symmetry imposed.

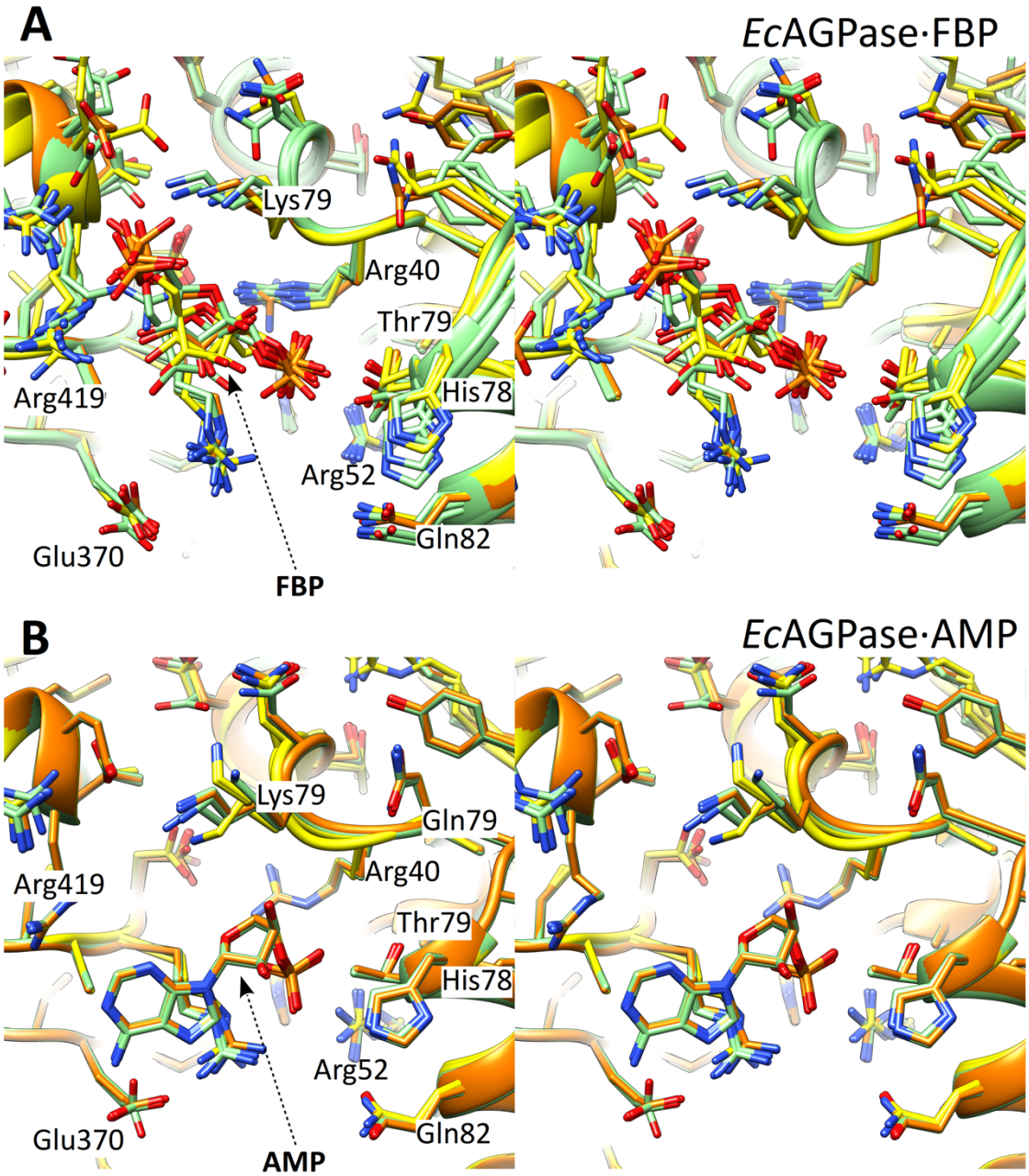

Figure S7. Local stereo views (crossed-eyes) of the allosteric cleft of *Ec*AGPase-FBP and *Ec*AGPase-AMP complexes. (**A**) Superposition of the D2 (orange), C2 (yellow), and C1 (green) models of the *Ec*AGPase-FBP complex showing the FBP ligand and the surrounding region. (**B**) Superposition of the D2 (orange), C2 (yellow), and C1 (green) models of the *Ec*AGPase-AMP complex showing the AMP ligand and the surrounding region.

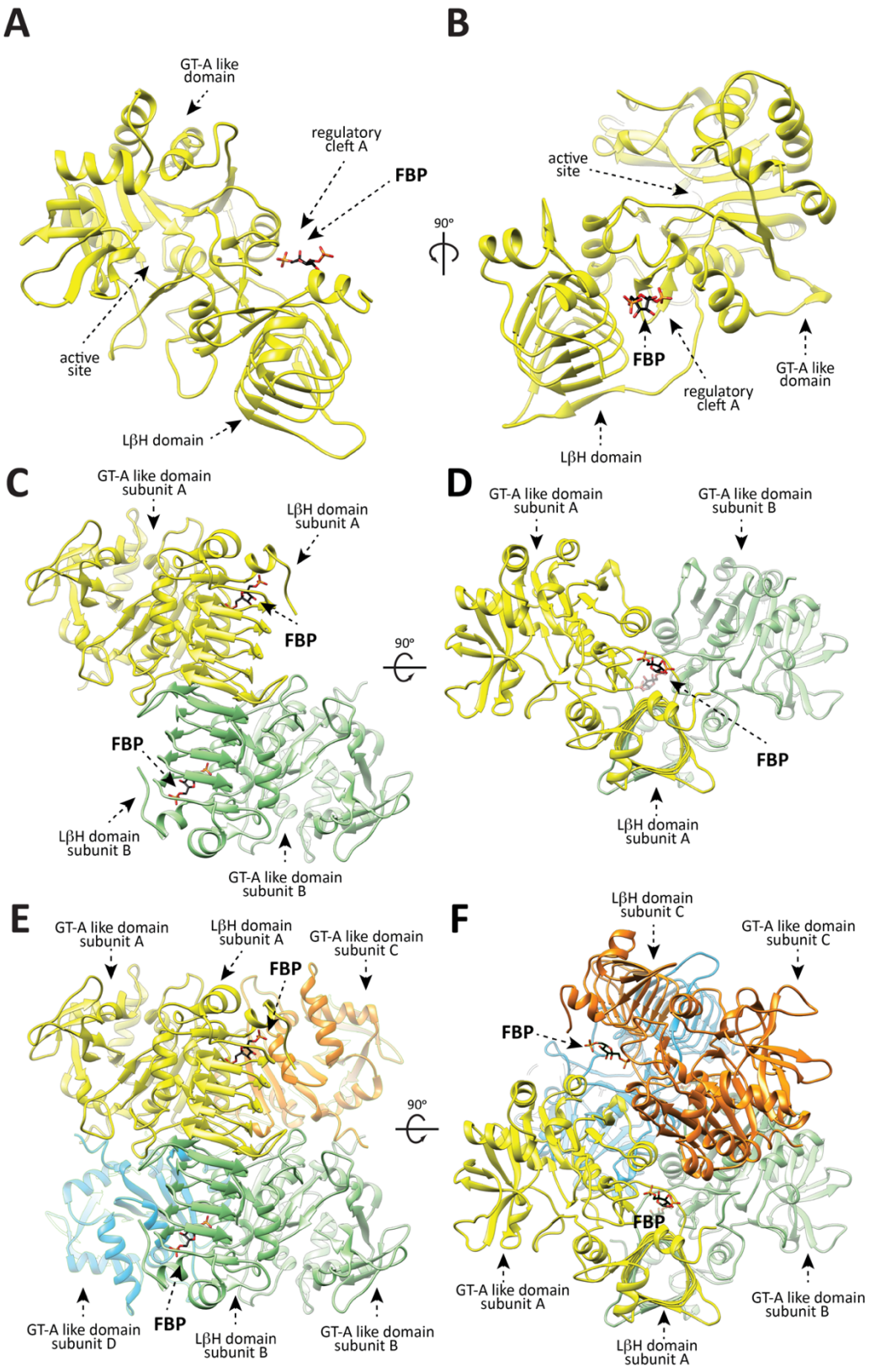

Figure S8. Overall structure of *Ec*AGPase as visualized by CryoEM. (**A**) Two views of an *Ec*AGPase protomer as visualized in the cryoEM *Ec*AGPase-FBP complex showing the GT-A-like domain and the LβH. (**B**) Two views of the *Ec*AGPase dimer. The protomers A and B are shown in yellow and green, respectively. (**C**) Two views of the *Ec*AGPase homotetramer. The protomers A, B, C and D are shown in yellow, green, orange and blue, respectively. The location of the active and regulatory sites is indicated.

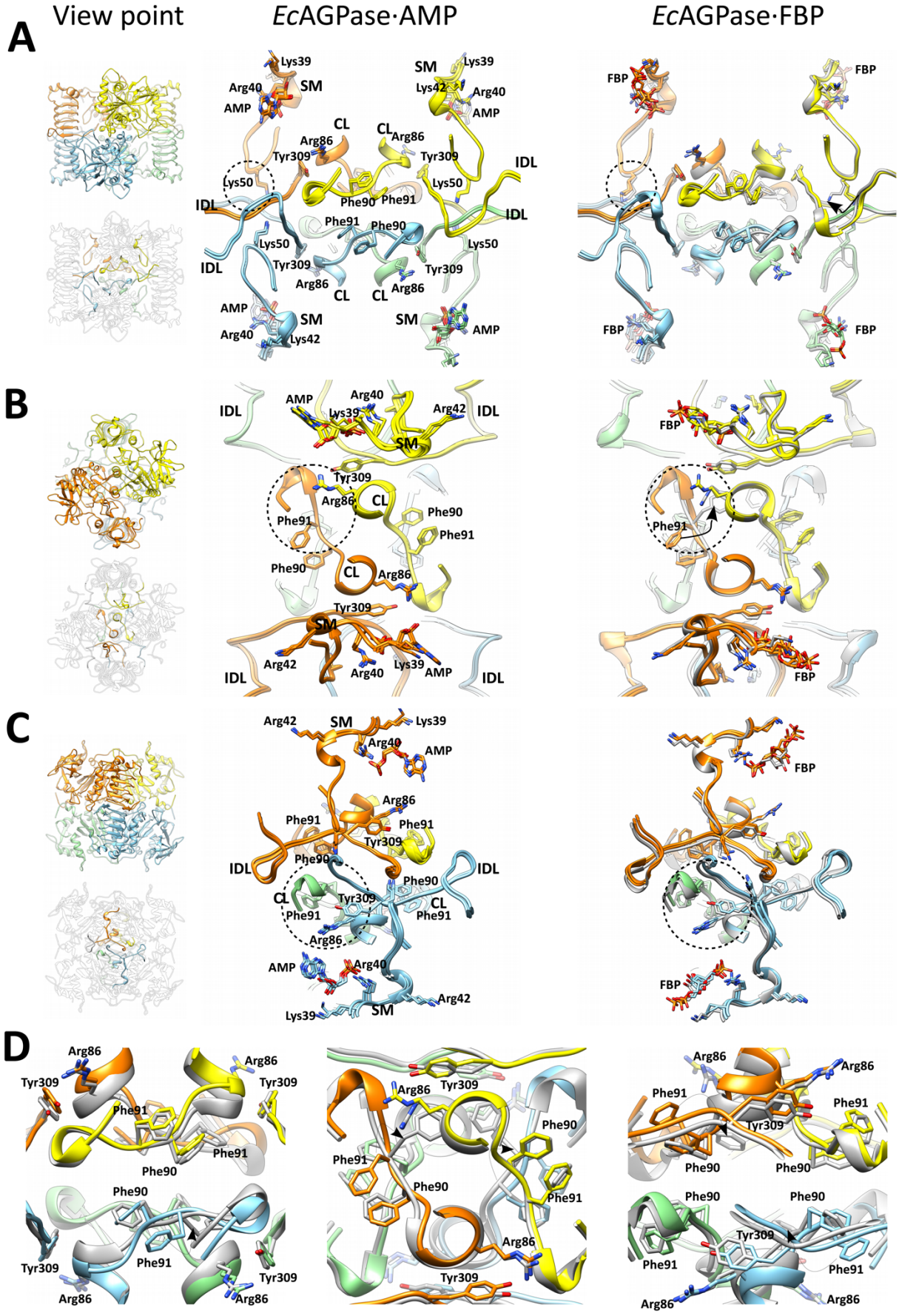
A
View point
EcAGPase·AMP
EcAGPase·FBP
Lys39
SM
Arg40
AMP
Lys42
CL
Arg86
Tyr309
IDL
Lys50
Phe90
Phe91
FBP
B
C
D

Figure S9. The SM, CL, and IDL in the *Ec*AGPase-FBP and *Ec*AGPase-AMP complexes in different symmetries. (**A-C).** Three views of the *Ec*AGPase-FBP and *Ec*AGPase-AMP complexes in different symmetries. From left to right: (*left*) structural view of the homotetramer showing the full-colored protomers as ribbons (*left-top*), and the SM, CL, and IDL in color with the rest of the structure as transparent ribbons (*left-bottom*); (*center*) close-up of the D2, C2, and C1 reconstruction models of *Ec*aGPAse-AMP complex, highlighting the SM, CL, and IDL; (*right*) close-up of the D2, C2, and C1 reconstruction models of the *Ec*aGPAse-FBP complex showing the SM, CL, and IDL. The D2 and C2 symmetries are in color, whereas the C1 symmetry is in grey. Critical structural elements and selected residues side chains are labeled in the *Ec*AGPase-AMP complex as reference. Note the high agreement of the *Ec*AGPase-AMP complex in different symmetries compared to that of the *Ec*AGPase-FBP complex. Discontinuous circles indicate local regions with high variability between *Ec*AGPase-AMP and *Ec*AGPase-FBP complexes. Arrows indicate the swing of side-chain residues between complexes and different symmetries. (**D**) Three orthogonal views of the superposition of the *Ec*AGPase-AMP D2 complex (color) with the *Ec*AGPase-FBP C1 complex (grey). The view is centered in the CL.

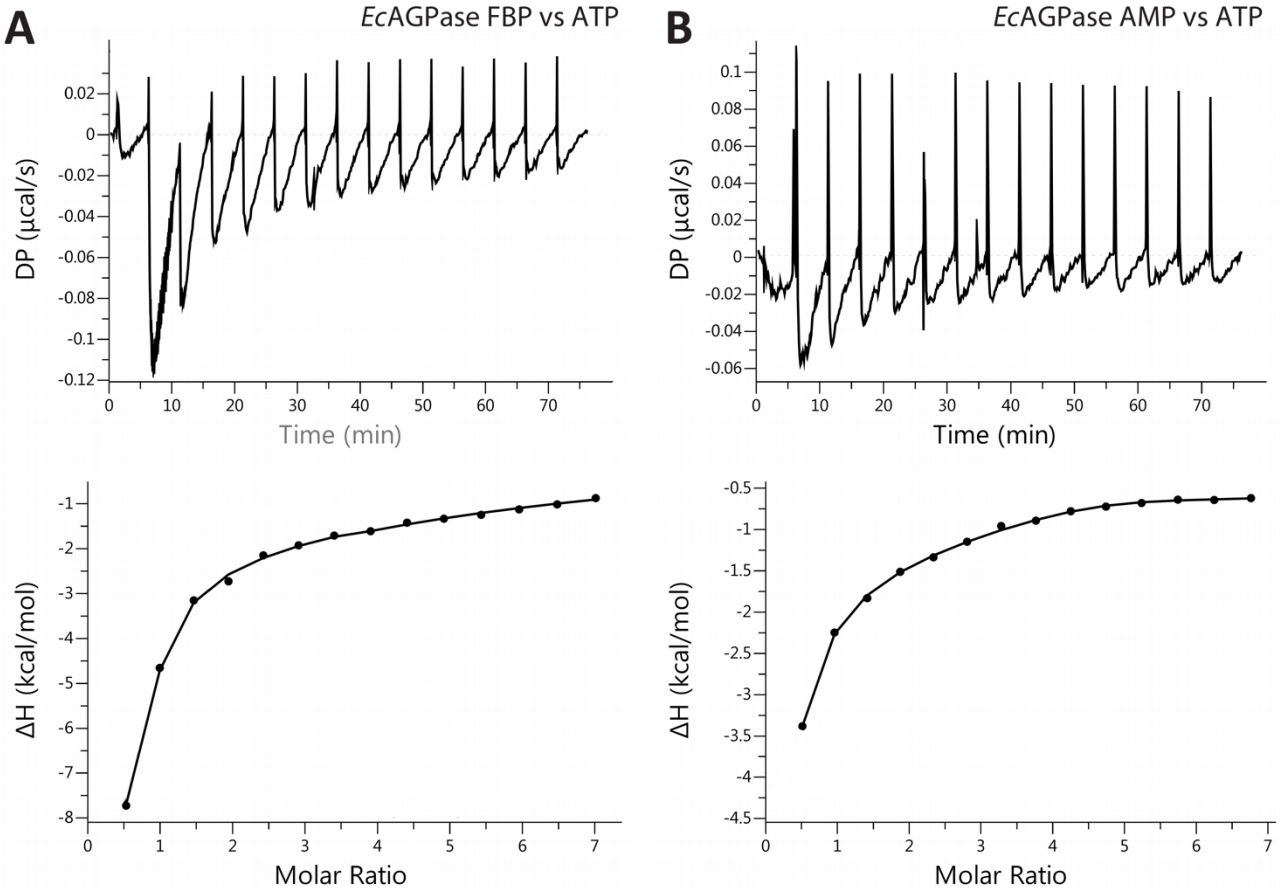

Figure S10. ITC measurements of *Ec*AGPase-FBP and *Ec*AGPase-AMP complexes with ATP. (**A**) The *upper panel* shows the raw data of the titration of the *Ec*AGPase-FBP complex with ATP. The lower panel shows the integrated heat of injections of the above titrations normalized per mol of ATP versus the molar ratio of ATP/*Ec*AGPase fitted to a sequential binding sites model. (**B**) The *upper panel* shows the raw data of the titration of the *Ec*AGPase-AMP complex with ATP. The lower panel shows the integrated heat of injections of the above titrations normalized per mol of ATP versus the molar ratio of ATP/*Ec*AGPase fitted to a sequential binding sites model.

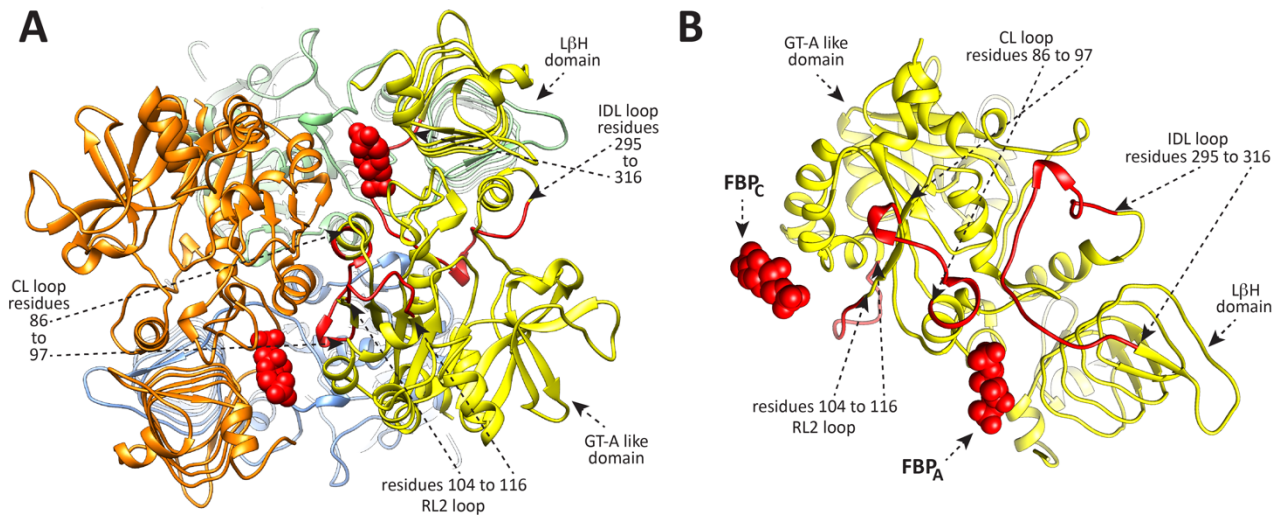

Figure S11. Allosteric residue interaction network (RIN) analyzed. (**A-B**) Two views of the *Ec*AGPase-FBP$_{D2}$ model showing the RINs analyzed.

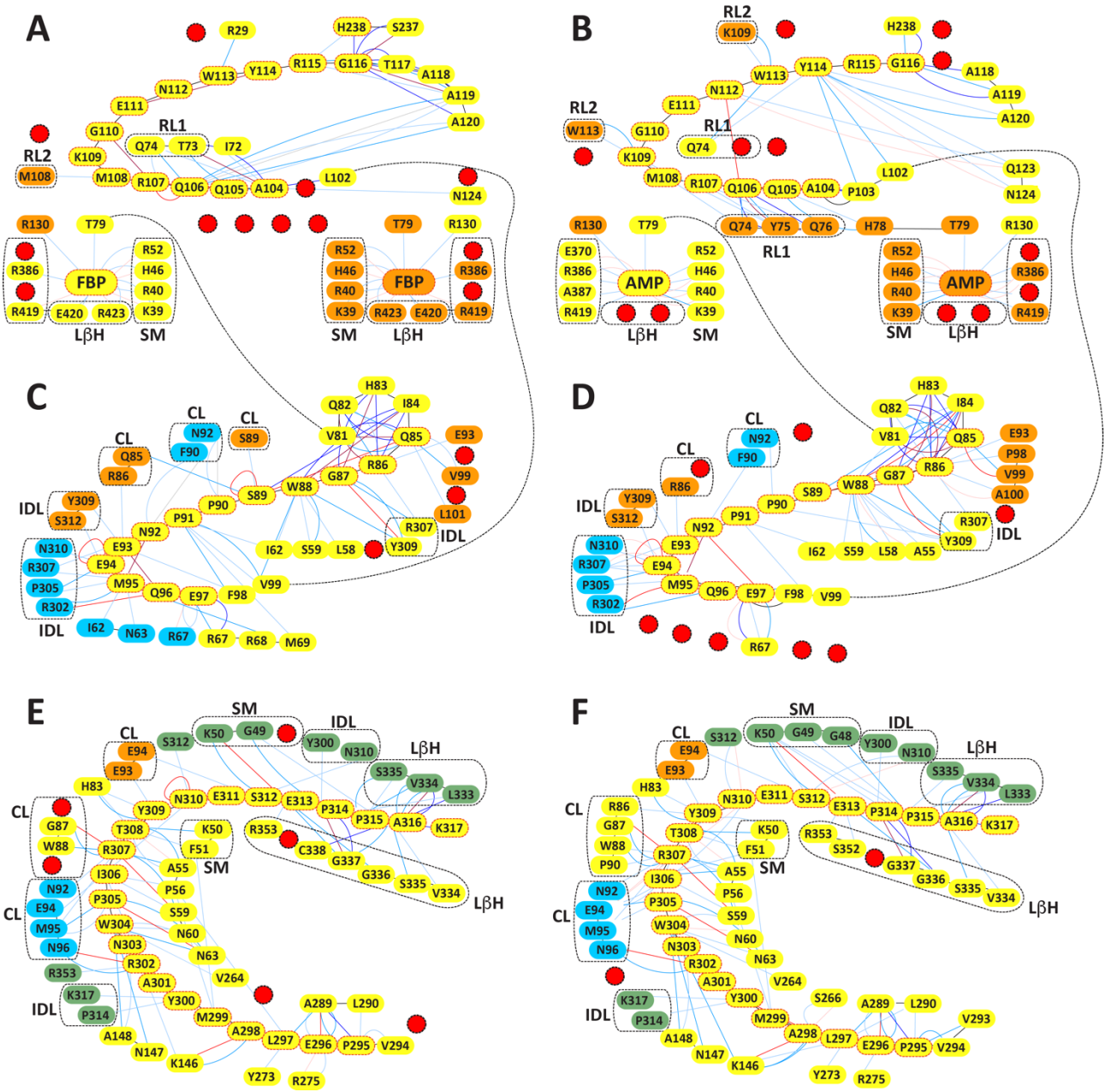

Figure S12. RIN differences between *Ec*AGPase-FBP and *Ec*AGPase-AMP complexes. (**A-B**). The RIN between the RL2 (104-116) and the corresponding allosteric regulator observed in the *Ec*AGPase-FBP_{D2} and *Ec*AGPase-AMP_{D2} complexes, respectively, are depicted as boxes highlighted in red. (**C-D**). The RIN between the CL (85-97) and the corresponding allosteric regulator observed in the *Ec*AGPase-FBP_{D2} and *Ec*AGPase-AMP_{D2} complexes, respectively, are depicted as boxes highlighted in red (**E-F**). The RIN between the IDL (104-116) and the corresponding allosteric regulator observed in the *Ec*AGPase-FBP_{D2} and *Ec*AGPase-AMP_{D2} complexes, respectively, are depicted as boxes highlighted in red. For panels (**A**) to (**F**), the interacting residues in other protomers are colored according to the panel (**A**) scheme described in Figure S9. The interactions are shown as straight or curved lines connecting residues. Interaction lines are colored according to different types of interactions as interatomic contacts (shades of blue), hydrogen bond (shades red), main chain bonds (black) and distant main chain connections (black dashed lines). Groups of residues from different elements are enclosed in black boxes. Red circles indicate missing residues in the interaction network between the *Ec*AGPase-FBP_{D2} and the *Ec*AGPase-AMP_{D2} models.

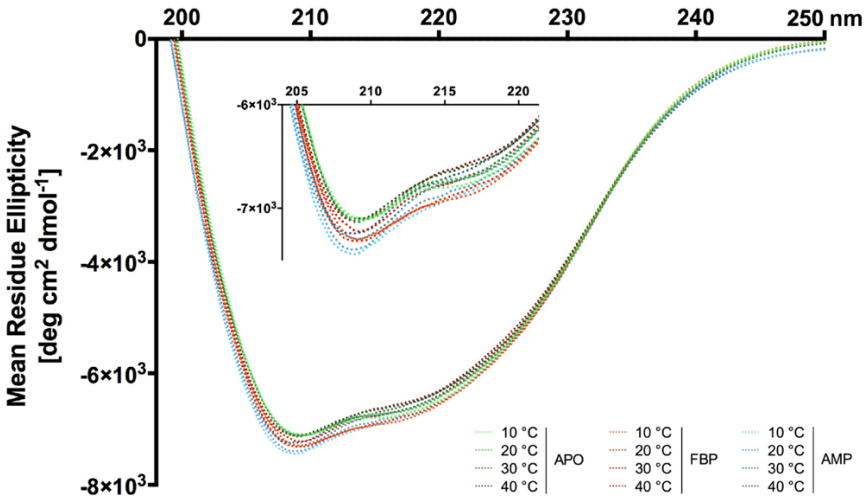

Figure S13. Circular dichroism spectrum of *Ec*AGPase in the absence or presence of regulators at different temperatures. The far-UV CD spectra were acquired at 10, 20, 30 and 40 ºC for the *Ec*AGPase in the apo state (green), in the presence of the negative regulator AMP (blue) and in the presence of the activator FBP (red). A close-up view of selected region of the spectra is shown for clarity.

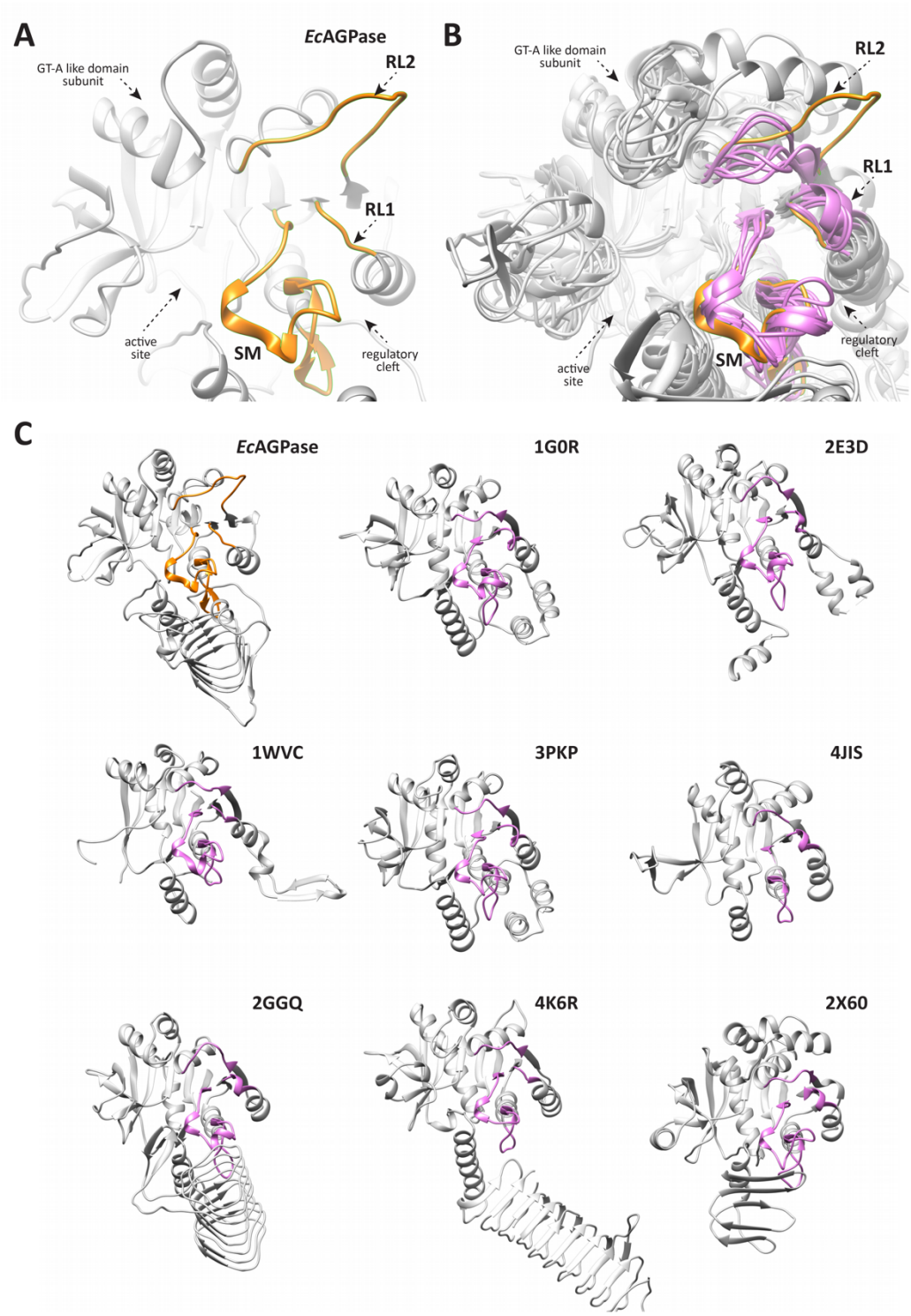

Figure S14. Structural superposition of *Ec*AGPase with other NDPases. (**A**) The cryoEM structure of *Ec*AGPase in complex with AMP, showing the position of the active site elements SM, RL1 and RL2 loops in the "locked" conformation in orange. (B) Structural superposition of selected NDPases highlighting equivalent active site elements referred in panel A, in pink. (C) Gallery of aligned NDPases structures labeled with their corresponding PDB accession codes; 1G0R: glucose-1-phosphate thymidyltransferase (RmlA) from *P. aeruginosa* in complex with G1P (EC:2.7.7.24); 2E3D: glucose-1-phosphate uridylyltransferase from *E. coli* (EC:2.7.7.9); 1WVC: glucose-1-phosphate cytidylyltransferase from *Salmonella enterica* complexed with cythidine-5'-triphosphate (EC: 2.7.7.33); 3PKP: glucose-1-phosphate thymidyltransferase from *S. enterica* (RmlA-Q83S variant) with 2'deoxy-adenosine triphosphate (EC:2.7.7.24); 4JIS: ribitol 5-phosphate cytidylyltransferase (TarI) from *Bacillus subtilis* (EC:2.7.7.40); 2GGQ: glucose-1-phosphate

thymidylyltransferase from *Sulfolobus tokodaii* in complex with TTP (EC:2.7.7.24); 4K6R: GlmU from *Mycobacterium tuberculosis* in complex with ATP (EC: 2.7.7.23); 2X60: GDP-manose pyrophosphorilase from *Thermotoga maritima* in complex with GTP (EC:2.7.7.13).

SUPPLEMENTARY MATERIALS AND METHODS

3.1. *Ec*AGPase purification

Overnight cultures of 100 ml of *Escherichia coli* BL21 transformed with the plasmid pET22b-*Ec*AGPase containing the full-length *Escherichia coli* K12 *glgC* gene were inoculated in 2L of LB medium supplemented with 100 mg L^{-1} carbenicillin and grow at 37 °C until cultures reached an A600 of 0.8.[16,30] Cultures were set to 18°C and *Ec*AGPase expression induced by the addition of 1 mM isopropyl-D-1-thio-galactopyranoside (IPTG) and incubated for 18-20 hs. Bacterial cells were harvested by centrifugation at 5,000 g and resuspended in 40 ml of 50mM HEPES pH 8.0, 10% w/v sucrose, 5 mM $MgCl_2$ and 0.1 mM EDTA (solution A). The cell suspension was supplemented with protease inhibitors (Pierce protease inhibitor mini tablets, Thermo Scientific), 10 mg L^{-1} of lysozyme (Sigma) and 2 µl of Benzonase (Merck), and incubated for 30 min on an ice bath. Subsequently, the suspension was sonicated and the cell lysate centrifuged for 20 min at 20,000 g. The supernatant was dialyzed two times against solution A, by using a 100 kDa MWCO cellulose dialysis membrane (Spectra/Por, Spectrum). The solution was applied to a 30 ml home packed Q-Sepharose Fast Flow column (GE Healthcare) previously equilibrated with solution A. The column was then washed with solution A until no absorbance at 280 nm was detected. *Ec*AGPase was eluted employing a linear gradient from 100% solution A to 100% solution B (solution A containing NaCl 0.5 M) in 100 ml. Fractions were tested for *Ec*AGPase activity as previously described.[16] The activite-positive fractions were then pooled. Solid ammonium sulfate was added to the suspension at room temperature to a calculated final concentration of 1.2 M. The resulting suspension was centrifuged at 32,000 g for 20 min, and the collected supernatant applied into a Phenyl HIC PH-814 column (Shodex) previously equilibrated in solution C (solution A containing ammonium sulfate 1.2 M). The enzyme was eluted from the column applying a linear gradient from 100% solution C to 100% solution A in 50 ml at a 1ml min^{-1} flow rate. Fractions with high-purity *Ec*AGPase, tested SDS-page, were pooled and dialyzed against solution A with a 100-kDa molecular overnight at 4ºC and stored at 80°C for subsequent experiments.

3.2. CryoEM sample preparation

An initial inspection by negative stain and cryoEM grid-screening and optimization was performed using an in-house Jeol 2200, 200 kV FEG equipped with an UltraScan 4000 CCD camera (Gatan, USA). Frozen aliquots of *Ec*AGPase in solution A where thawed and concentrated to 4 mg ml^{-1}. Samples of 50 µl of *Ec*AGPase were injected in an analytical SEC column KW-403-F (Shodex) previously equilibrated with 50 mM Tris-HCl pH 7.5, 100 mM NaCl and 2 mM $MgCl_2$, and the protein peak collected in 50 µl fractions for subsequent vitrification. The *Ec*AGPase-AMP sample was obtained by mixing SEC protein fractions at 0.6 mg/ml with an equal volume of a solution of 0.5 mM AMP in 50 mM Tris-HCl, pH 7.5 and 100 mM NaCl. The resulting solution containing *Ec*AGPase 0.3 mg ml^{-1} and 0.25 mM AMP was applied onto copper Quantifoil R 1.2/1.3 grids. Grids were plunge-freeze into liquid ethane using a Vitrobot MkII (FEI) at 10ºC and 80 HR% humidity in the chamber (Figure S3). The *Ec*AGPase-FBP complex was obtained mixing equal parts of *Ec*AGPase at 0.6 mg ml^{-1} with 5 mM FBP in 50 mM Tris-HCl pH 7.5 and 100 mM NaCl. The resulting solution containing *Ec*AGPase 0.3 mg ml^{-1} and 2.5 mM FBP was applied onto home-made graphene oxide coated copper Quantifoil R 1.2/1.3 grids using a Vitrobot MkII (FEI) at 10ºC and 80 HR% humidity in the chamber (Figure S2).

Home-made graphene oxide grids were made with a smith grid coating trough (LAAD research industries) in which the perforated metal tray was centrally covered with a strip of 1 cm wide Parafilm (Bemis). The device was filled with Milli-Q water until the tray was covered entirely. Grids were immersed in the water and the grids placed on top of the Parafilm, with the carbon side up. A suspension of graphene oxide was made by vortexing 100 µl of graphene oxide at 2 mg ml^{-1} (Sigma) with 100 µl of methanol. The suspension was added drop-by-drop onto the water surface and incubated for 1 min. The liquid in the smith grid coating trough was removed by aspiration with a syringe leaving a drop of water with graphene stayed on top of the grids. The tray with the grids was deposited in a petri dish with filter paper and leave inside a desiccator overnight for next day use.

3.3. CryoEM data collection

Data were collected at the Electron Bio-Imaging Centre (eBIC) at Diamond Light Source, Oxfordshire, UK. The data of both *Ec*AGPase-FBP and *Ec*AGPase-AMP complexes were acquired using the Titan Krios-I (FEI) operated at 300 kV (Cs 2.7 mm). Data was recorded using a Quantum K2 Summit camera (Gatan) in counting mode, recording 40 frames/movie at a final pixel size of 1.047 Å. Automatic data collection was performed using the software EPU 1.9.1 (FEI; Table 1 and Figures S2 and S3).

3.4. CryoEM single-particle data processing

*Ec*AGPase-AMP and *Ec*AGPase-FBP complexes data set were processed using the general protocol described in the following lines. Data processing was initiated using the Relion 3.0 suite.[56] The 40 movie frames of each movie were aligned using MotionCor2 (5x5 patches and Bfactor 150). The CTF of the aligned image was assessed in the non-dose weighted image using CtfFind 4.1 with parameters amplitude contrast 10% and FFT box size of 512 pixels. Image CTF was visually inspected, and images with low quality discarded. Relion reference-free automatic particle picking was performed considering a particle diameter between 95 Å and 110 Å, imposing a minimum inter-particle distance of 90 Å and a low picking threshold (0.05). Extracted particles were extracted using a square box of 200 pixels side. Particles were subjected to several rounds and extensive 2D classification selecting the best classes. An initial first 3D auto-refinement in C1 was performed using a calculated map at 35 Å resolution produced in USCF-Chimera[57,58] from the *Ec*AGPase tetramer from the crystal structure (pdb code PDB 5L6S). This initial reconstruction was used to re-extract centered particles. Afterward, several steps of 3D classification in C1 were performed to discarding bad classes until models reached resolutions better than 6Å and visual inspection revealed a well-defined tetrameric structure. The selected 3D classes were used to reconstruct a model using Relion 3D auto-refinement protocol in C1, which led to a map resolving better than Å. This reconstruction was used as a starting

point to perform one round of Relion CTFrefinement and particle Polishing. Later, polished and CTF-refined particles from Relion were imported into CryoSparc2 and a final 2D classification of 200 classes was performed and the best-defined classes selected (Figures S2B and S3B). Final 3D reconstructions were performed in CryoSparc2 using the homogeneous refinement imposing C1, C2 and D2 symmetry and applying dynamic masking, using the Relion reconstructions low-pass at 30 Å as starting model. Finally, a final step of Non-Uniform refinement for each reconstruction, on the corresponding symmetry, was performed applying a calculated global mask from each reconstruction. The reconstructions obtained from the non-uniform CryoSparc2 protocol are reported for each symmetry. Reported auto sharp-maps were obtained from the CryoSparc2 non-uniform refinements (Figures S2C and S3C). Local resolution was measured in CryoSparc2 LocRes program implementation,[59] using a threshold for local FSC = 0.5 for local resolution assesment (Figures S2C and S3C). For quality graphs as FSC plots, angular distribution and precision see (Figures S2D-F and S3D-F). For other statistics please see Table 1.

3.5. Model building and refinement

A model of the *Ec*AGPase tetrameter without ligands and trimmed RL1 and RL2 loops from the X-ray crystal structure (pdb code PDB 5L6S), was initially rigid-body fitted inside the cryoEM reconstruction using chimera.[57] The refinement of the models using Phenix real space_refinement[60,61] in the sharp maps was performed with alternative rounds of Coot modeling[62] for and de-novo loop building. Corresponding NCS were enforced for model refinement in the D2 and C2 map reconstructions, meanwhile, automatic NCS determination was used in the C1 reconstruction. The quality of models was checked during refinements using Molprobity and validate-PDB server.[63] For model statistics and quality details please see Table 1.

3.6. Visualization, structural analysis and bioinformatics

Analysis of the structures and density maps, morphing, sequence alignments, images, and

visualization was done using UCSF Chimera. Residue interaction networks analysis was performed using RINalyzer program on Cytoscape. The multiple sequence alignment was performed using UNIPROT online service using Clustal Omega (1.2.4). The aligned AGPase sequences were retrieved from UNIPROT: *Escherichia coli* (P0A6V1), *Triticum aestivum* (P30523), *Arthrobacter sp.* (A0JWV0), *Haemophilus influenzae* (P43796), *Klebsiella pneumoniae* (B5XTQ9), *Enterobacter sp.* (A4WFL3), *Nostoc punctiforme* (B2IUY3), *Rhodobacter sphaeroides* (A3PJX6), *Rhodospirillum rubrum* (Q2RS49), *Rhizobium radiobacter* (P39669), *Solanum tuberosum* (P23509), and *Cronobacter sakazi* (A7MGF4). Conservation scores reported in Table 2 were obtained from Jalview conservation histogram.[64,65]

3.7. Thermofluor

*Ec*AGPase frozen aliquots were thawed and buffer exchanged in 50 mM Tris-HCl pH 7.5, 100mM NaCl and concentrated to obtain a protein stock of 4mg ml^{-1}. The thermofluor assay was performed in a total reaction volume is 25 µl as follows. First, a volume of 20 µl of an assayed mix of ligands in 50 mM Tris-HCl pH 7.5, 100mM NaCl to obtain corresponding final concentrations of either AMP 0.5 mM, FBP 2.5 mM, and/or ADP-glucose 0.5 mM was deposited onto 96-well thin-wall PCR plate (Hardshell, Bio-Rad) in an ice bath. Secondly, 2.5 µl of a 1:100 dilution in water of the probe SYPRO Orange stock (S5692, Sigma) to each well. Finally, 2.5 µl of protein stock or buffer was added corresponding wells to measure protein and controls in triplicates. The reaction plate was covered with transparent adhesive sealer (Microseal, Bio-Rad) and kept on ice bath until measurement. The experiment was performed in a CFX96 qPCR System Thermocycler (Bio-Rad), with the block pre-cooled at 4ºC and the lid pre-heated to 98ºC. The experiment was run using a ramping temperature from 4ºC to 95ºC with an increment of 1ºC min^{-1} and data measured in the HEX channel. Well-to-well baseline differences between curves were corrected by subtraction their corresponding fluorescence value at the denaturation peak maxima, as considering the fluorescence value at the denaturation peak maxima should be constant to the interaction probe-protein in a given condition.

Therefore, the resulting corrected curves with fluorescence value at the denaturation peak maxima equals 0. Corrected curve triplicates were averaged, and the signal from buffers subtracted.

3.8. Isothermal titration calorimetry

To study of binding differences for ATP to *Ec*AGPase in the presence of allosteric regulators was carried out at 25 °C in the presence of 2 mM $MgCl_2$ using a MicroCal PEAQ-ITC calorimeter (Malvern Pananalitycal). Specifically, the 20 uM *Ec*AGPase in buffer 100 mM NaCl, 200 mM Tris-HCl pH 7.5 with either AMP 0.1 mM or FBP 2.5 mM was titrated with 14 injections of 2.5 µl of ATP 1 mM in matching buffer with an equilibration time of 300 s/injection. Protein buffers were treated in the same fashion to assess the dilution heat of ATP. Data from protein experiment was subtracted with the control buffers and was fitted imposing a model for four sites sequential binding site using the MicroCal PEAQ-ITC analysis software where: K_{D1}=[*Ec*AGPase][ATP]/[*Ec*AGPase-ATP_1]; K_{D2}=[*Ec*AGPase-ATP_1][ATP]/[*Ec*AGPase-ATP_2]; K_{D3}=[*Ec*AGPase-ATP_2][ATP]/[*Ec*AGPase-ATP_3]; K_{D4}=[*Ec*AGPase-ATP_3][ATP]/[*Ec*AGPase-ATP4].

3.9. Far-UV Circular Dichroism spectra and thermal unfolding

*Ec*AGPase frozen aliquots in solution A thawed and concentrated to 4mg/ml. These samples were buffer exchanged by size-exclusion chromatography (Superdex 200 10/300 GL, GE) into buffer 10 mM Tris pH 7.5 100 mM NaF (CD buffer). Protein fractions of the single peak corresponding to the EcAGPase tetramer were pooled to a final concentration of 0.6 mg/ml. Samples were prepared by mixing equal parts of 0.6 mg/ml protein solution with CD buffer with either 0.2 mM AMP, 5 mM FBP, or without regulators. The CD spectra in the far UV region (250-190 nm) were measured utilizing a J-815 CD spectrometer (Jasco), by using a 1 mm path length High Precision Cell cuvette (Hellma). To explore the ligand effects in a range of physiological temperatures, 20 accumulations of each spectrum were recorded for each sample at 10, 20, 30 and 40 ºC. Spectra were normalized by subtracting the buffer spectra from the raw data. Data were converted from mdeg to Mean Residue

Ellipticity $[\theta]_{MRW,\lambda}$ according to the formula "$[\theta]_{MRW,\lambda} = \theta$.MRW/10.d.c", where θ is the observed ellipticity (degrees), MRW is the molecular mass divided by N-1, with N as the number of amino acids, d is the optical path (cm), and c is the concentration in g/ml.

3.10. Qualitative meta-analysis of *Ec*AGPAse single point mutants

To simplify the examination of reported kinetic properties of *Ec*AGPase single-point mutants, we approach the meta-analysis only for single point mutations of residues at the active site and the regulatory cleft to alanine residues (Table 2).[32,37,38] In addition, to set the basis for the comparison across different reports, we standardized mutant values as a ratio against the corresponding wild-type value reported in each individual study, i.e. Vmax-ratio = mutantVmax/wild-typeVmax. Finally, for the benefit of a qualitative characterization of these mutants, we perform an *ad-hoc* classification into three groups with marked differences: (i) mutants with parameter between the half and the double of the values displayed by the wild-type enzyme (0.5> parameter mutant/wild-type < 2.0, symbolized as "~" in Table 2), (ii) mutants with high ratio (parameter mutant/wild-type > 2.0, symbolized as "↑" in Table 2), and (iii) mutants with low ratio (parameter mutant/wild-type < 0.5 , symbolized as "↓" in Table 2).

SUPPLEMENTARY REFERENCES

[56] J. Zivanov, TNakane, B.OForsberg, D. Kimanius, W.J. Hagen, E. Lindahl, S.H. Scheres, New tools for automated high-resolution cryo-EM structure determination in RELION-3, *Elife* (2018) e42166.

[57] E.F. Pettersen, T.D. Goddard, C.C. Huang, G.S. Couch, D.M. Greenblatt, E.C. Meng, T.E. Ferrin, UCSF Chimera--a visualization system for exploratory research and analysis, J. Comput. Chem. 25 (2004) 1605–1612.

[58] S.J. Ludtke, P.R. Baldwin, W. Chiu, EMAN: semiautomated software for high-resolution single-particle reconstructions, J. Struct. Biol. 128 (1999) 82–97.

[59] G. Cardone, J.B. Heymann, A.C. Steven, One number does not fit all: mapping local variations in resolution in cryo-EM reconstructions, J. Struct. Biol. 184 (2013) 226–236.

[60] P.D. Adams, et al. PHENIX: a comprehensive Python-based system for macromolecular structure solution, Acta Crystallogr. D. Biol. Crystallogr. 66 (2010) 213–221.

[61] P.V. Afonine, B.K. Poon, R.J. Read, O.V. Sobolev, T.C. Terwilliger, A. Urzhumtsev, P.D. Adams, Real-space refinement in PHENIX for cryo-EM and crystallography, Acta Crystallogr. D. Biol. Crystallogr. 74 (2018) 531–544.

[62] P. Emsley, B. Lohkamp, W.G. Scott, K. Cowtan, Features and development of Coot, Acta Crystallogr. D. Biol. Crystallogr. 66 (2010) 486–501.

[63] V.B. Chen, et al. MolProbity: all-atom structure validation for macromolecular crystallography. Acta Crystallogr. D. Biol. Crystallogr. 66 (2010) 12–21.

[64] A.M. Waterhouse, J.B. Procter, D.M. Martin, M. Clamp, G.J. Barton. Jalview Version 2--a multiple sequence alignment editor and analysis workbench. Bioinformatics (2009) 25, 1189–1191.

[65] C.D. Livingstone, G.J. Barton. Protein sequence alignments: a strategy for the hierarchical analysis of residue conservation. Comput. Appl. Biosci. (1993) 9, 745–756.